

**Insight into the limited electrochemical activity of NaVP207**

Journal:	<i>RSC Advances</i>
Manuscript ID:	RA-ART-06-2015-012158.R1
Article Type:	Paper
Date Submitted by the Author:	19-Jul-2015
Complete List of Authors:	Kee, Yongho; Kyushu University, Interdisciplinary Graduate School of Engineering and Sciences Dimov, Nikolay; Kyushu University, Interdisciplinary Graduate School of Engineering and Sciences; Kyushu University, Institute for Materials Chemistry and Engineering Kasuga Staykov, Aleksandar; Kyushu University, International Institute for Carbon Neutral Energy Research Barpanda, Prabeer; Indian Institute of Science, Materials Research Centre Lu, Ying-Ching; Kyushu University, Interdisciplinary Graduate School of Engineering and Sciences Minami, Keita; Kyushu University, Interdisciplinary Graduate School of Engineering and Sciences Okada, Shigeto; Kyushu University, Institute for Materials Chemistry and Engineering

Insight into the limited electrochemical activity of NaVP_2O_7

Yongho Kee^a, Nikolay Dimov^b, Aleksandar Staikov^c, Prabeer Barpanda^{b,d}, Ying-Ching Lu^a, Keita Minami^e, and Shigeto Okada^{b,†}

^aInterdisciplinary Graduate School of Engineering Sciences, Kyushu University, 6-1, Kasuga-koen, Kasuga 816-8580, Japan

^bInstitute for Materials Chemistry and Engineering, Kyushu University, 6-1, Kasuga-koen, Kasuga 816-8580, Japan

^cInternational Institute for Carbon-neutral Energy Research (WP1-12CNER), Kyushu University, 744 Motooka, Nishi-ku, Fukuoka, 819-0395, Japan

^dFaraday Materials Laboratory, Materials Research Centre (MRC), Indian Institute of Science, C.V. Raman Avenue, Bangalore 560012, India

^eElements Strategy Initiative for Catalysts and Batteries (ESICB), Kyoto University, Katsura, Kyoto 615-8520, Japan

[†]Corresponding author. Tel: +81925837841, Fax: +81925837841

Email: s-okada@cm.kyushu-u.ac.jp (S.Okada)

Abstract

Recently, LiVP_2O_7 has been investigated as a possible high-voltage substitute for $\text{Li}_2\text{FeP}_2\text{O}_7$. However, its Na-equivalent, NaVP_2O_7 , as an economic replacement for $\text{Li}_2\text{FeP}_2\text{O}_7$ has not yet been well understood. Here, for the first time, we report the feasibility of NaVP_2O_7 as a 3.4 V cathode material for Na-ion battery. Having a theoretical capacity of $108 \text{ mAh}\cdot\text{g}^{-1}$, it shows an initial discharge capacity of $38.4 \text{ mAh}\cdot\text{g}^{-1}$ at $1/20 \text{ C}$ ($1\text{C} = 108 \text{ mA}\cdot\text{g}^{-1}$) in the voltage range of 2.5-4.0 V. Our study suggests that part of the sodium ions in the lattice structure exists as structural stabilizer and brings lattice distortion upon desodiation. This study also shows that the title compound, NaVP_2O_7 , suffers from high intrinsic internal resistance, which limits the phase transition kinetics between pristine NaVP_2O_7 and desodiated $\text{Na}_{1-x}\text{VP}_2\text{O}_7$.

Keywords: Sodium-ion batteries, pyrophosphate, NaVP_2O_7 , lattice distortion, migration barrier energy

1. Introduction

Polyanionic host materials such as LiMPO_4 , $\text{Li}_x\text{M}_2(\text{PO}_4)_3$, Li_xMSiO_4 , and $\text{Li}_2\text{MP}_2\text{O}_7$ have been widely explored and implemented as promising Li-ion battery electrode materials due to their high thermal stability and the inductive effect of the hetero atoms in the polyanion group, which effectively increases the operating voltage of transition metal redox couples.¹⁻⁹ However, limited availability of Li-containing minerals considerably restricts the adoption of lithium-ion batteries in the large-scale energy storage systems. One of the promising alternatives to current Li-ion secondary batteries are Na-ion batteries, which have potential price competitiveness due to the abundance of Na in the nature. So far, many Na-ion battery host materials were rooted from their well-known Li-equivalents such as NaMPO_4 , $\text{Na}_x\text{M}_2(\text{PO}_4)_3$, and $\text{Na}_2\text{MP}_2\text{O}_7$ with promising electrochemical performances.¹⁰⁻¹² The overall operational principle of the lithium-ion and sodium-ion batteries is the same, i.e. reversible (de)insertion of the Li^+ or Na^+ between the cathode and the anode. With the suitable selection of electrolytes and anodes, the sodium-ion technology could be considered as borrowed from lithium-ion energy storage systems. Nevertheless, due to the larger ionic size of sodium relative to lithium, crystallographic symmetries and electrochemical performance of Na-based electrode materials are in most of the cases different from those of their Li-equivalents, which impose a huge driving force for exploration of other Na-containing novel electrode materials.^{11,13-17} Especially, these differences make the polyanionic sodium hosts interesting subject for fundamental investigations, where the comparison between isocompositional Li-ion and Na-ion hosts depicts interesting behavior with wide contrast.

Exploring phosphate-based polyanionic systems, recently $\text{Li}_2\text{FeP}_2\text{O}_7$ has been investigated as a potential cathode material with high theoretical capacity of $220 \text{ mAh}\cdot\text{g}^{-1}$ through two electron reactions involving two redox pairs: $\text{Fe}^{3+}/\text{Fe}^{2+}$ and $\text{Fe}^{4+}/\text{Fe}^{3+}$.¹⁸⁻¹⁹ However, the instability of high redox potential $\text{Fe}^{4+}/\text{Fe}^{3+}$ couple limits its practical capacity close to that of LiVP_2O_7 ,²⁰ having slightly higher operating voltage of $\text{V}^{4+}/\text{V}^{3+}$ redox pair (vs. Li). To the best of our knowledge, electrochemical properties of its Na-equivalent, NaVP_2O_7 with theoretical capacity of $108 \text{ mAh}\cdot\text{g}^{-1}$, have not yet been reported in the literature. If NaVP_2O_7 could show comparable electrochemical properties to its Li-equivalent, it would qualify as a promising cathode material for sodium-ion batteries. The current study aims to evaluate the feasibility of NaVP_2O_7 as a cathode material for Na-ion secondary batteries and explore its intrinsic electronic property upon partial desodiation by synergizing experimental study and theoretical calculations.

2. Experimental

A stoichiometric mixture of the commercial precursors, NaH_2PO_4 (Wako), NH_4VO_3 (Wako), $(\text{NH}_4)_2\text{HPO}_4$ (Wako), and citric acid (10% by the weight of the precursors) acting as a reducing agent, was ball-milled at 250 rpm for 1 h. This mixture was sintered at 800°C for 12 h under steady Ar-flow. Powder XRD pattern of NaVP_2O_7 was recorded by a Rigaku X-ray diffractometer (Cu-K α , 50kV, 300mA) in the 2θ range of 10 - 90° at a scan rate of $0.09^\circ/\text{min}$ (step size of 0.02°) and was refined by the Fullprof Suite refinement program using atomic coordinates obtained from the previously reported NaVP_2O_7 .²¹

In our preliminary research, the electrode pellets prepared via mild ball-milling (e.g. 1 h) showed almost no electrochemical activity. Therefore, in this study a mixture of 70 wt% electrode active material and 25 wt% acetylene black was ball-milled for 12 h at 550 rpm before 5 wt% of polytetrafluoroethylene (PTFE) binder was added to prepare electrode pellets. The average weight of each pellet was approximately 5 mg. These electrodes were vacuum-dried at 100 °C for 24 h to remove traces of water. 2032 coin cells were assembled in Ar-filled glove box (MBRAUN, Germany) with frost point below -100°C and oxygen content less than 1 ppm. All electrodes were cycled against Na metal using 1M NaPF₆ in PC:FEC (95:5 in volume) electrolyte at various C-rates (1C = 108 mA.g⁻¹) in the voltage range between 2.5V and 4.0 V. The morphology of the pristine and partially desodiated NaVP₂O₇ samples was observed by Field emission electron microscope (FE-TEM, JEM-2100F). Electrochemical impedance spectroscopy (EIS) was recorded in the frequency range between 100 kHz and 0.01 Hz at room temperature before the galvanostatic cycling and after 20th cycles with an AC signal of 10 mV to investigate intrinsic resistances.

X-ray photoelectron spectra (XPS, JPS-9010MC/IV) were recorded using excitation radiation of Mg-K_α (1253.6 eV) to investigate atomic environments of phosphorus and vanadium and fitted by CasaXPS software. To investigate changes in pyrophosphate groups, pristine NaVP₂O₇ before galvanostatic cycling, and the electrode pellets taken out after initial charging and discharging were dried for 24 h and ground with KCl powder (95:5 in weight) before their transmittances were recorded using Attenuated total reflectance Fourier transform infrared (ATR-FTIR, FT/IR-680 Plus) spectrometer.

To understand the possible structural variations of NaVP₂O₇, periodic plane wave density functional theory calculations were performed using Vienna *ab initio* simulation package (VASP) within the projector augmented-wave approach using the Perdew-Burke-Ernzerhof generalized-gradient approximation (GGA) functional.²²⁻²³ Perdew-Burke-Ernzerhof parameterization of the generalized gradient approximation (GGA-PBE) was employed using projector-augmented wave (PAW) pseudopotentials with an electron cutoff energy of 400 eV. (3x3x3) Monkhorst-Pack k-point sampling was used in the calculations. The energy barrier of single vacancy-assisted Na-ion diffusion between two closest Na-ions was calculated by the nudged elastic band (NEB) method.²⁴

3. Results and Discussion

3.1. Structural characterization

The XRD powder diffraction pattern of the solid-state synthesized title compound (NaVP₂O₇) matches well with the previously reported data²¹ without any distinct impurity and adopts the space group of *P2₁/c* (*Z* = 4) (**Fig. 1**). The background of XRD profile was fitted with linear interpolation between a set of 63 points with refinable heights and the peak shape was refined with the convolution of a pseudo-Voigt function. The atomic coordinates obtained from previously reported data²¹ were adopted for the structure refinement. The refinement was carried out until satisfactory *R_B* of 6.54% and *R_{wp}* of 10.23% were obtained with the cell parameters of *a* = 7.3169(2) Å, *b* = 7.9350(2) Å, *c* = 9.567(2) Å, *β* = 111.905(2) °, and *V* = 515.4(2) Å³ as illustrated in **Fig. 1**. NaVP₂O₇ is comprised of VO₆ octahedra linked together with five unique P₂O₇ groups, making narrow bottleneck channels for Na-ions to reside in. It has slightly distorted MO₆ octahedra, which is in good

agreement with its previously reported isostructures, NaMoP_2O_7 and $\beta\text{-NaTiP}_2\text{O}_7$.²⁵⁻²⁶ Another notable feature of NaVP_2O_7 ($V_m = 77.6 \text{ cm}^3 \text{ mol}^{-1}$) is that it crystallizes in the high symmetric space group of $P2_1/c$ similar to other AVP_2O_7 [$A = \text{K}$ ($V_m = 87.5 \text{ cm}^3 \text{ mol}^{-1}$, ICSD #68625), Rb ($V_m = 90.2 \text{ cm}^3 \text{ mol}^{-1}$, ICSD #300101), Cs ($V_m = 93.5 \text{ cm}^3 \text{ mol}^{-1}$, ICSD #65678)] family of compounds, while LiVP_2O_7 ($V_m = 77 \text{ cm}^3 \text{ mol}^{-1}$, ICSD #80551) and VP_2O_7 ($V_m = 74.6 \text{ cm}^3 \text{ mol}^{-1}$, ICSD #93022) crystallize in less symmetric space group of acentric $P2_1$.²⁷ This observation indicates that competitively large alkali metal A^+ (Na , K , Rb , Cs) in this lattice structure could exist as structural stabilizer of centrosymmetric $P2_1/c$ and NaVP_2O_7 could undergo irreversible phase transformation to acentric $P2_1$ and/or may coexist as two separate phases when Na -ions are partially reacted during charge and discharge processes. If this assumption is correct, the title compound, NaVP_2O_7 , may show electrochemical properties different from previously reported $\text{Na}_2\text{FeP}_2\text{O}_7$ and $\text{Na}_2\text{MnP}_2\text{O}_7$ with the lowest centric space group of $P-1$.^{12, 28-29}

3.2. Electrochemical properties

Although NaVP_2O_7 has been known to chemists for over two decades, surprisingly there has been no report on its electrochemical (de)sodiation behavior. In this study, the partial extraction of Na^+ from the title compound with good reversibility was observed as depicted by the charge/discharge profiles of NaVP_2O_7 vs. Na (**Fig. 2**). The working cell showed initial discharge capacity of $38.4 \text{ mAh}\cdot\text{g}^{-1}$ at $1/20 \text{ C}$ ($1\text{C} = 108 \text{ mA}\cdot\text{g}^{-1}$) in the voltage range of 2.5-4.0 V with the average $\text{V}^{4+}/\text{V}^{3+}$ redox potential centered at 3.4 V (vs. Na/Na^+). The steep recharge curve of NaVP_2O_7 can be attributed to the prolonged solid-solution

regions due to the reduction of miscibility gap between the sodiated and the desodiated phases.³⁰⁻³² The morphology of carbon-coated and desodiated electrode pellet of NaVP₂O₇ observed by FE-TEM is illustrated in **Fig. 3**. Fine nanoscale particles in the size range of 20-60 nm are observed with a thin coating of carbon. This formation of nanoscale morphology with carbon coating is suitable for enabling the electrochemical activity of target phase. The Nyquist plots obtained from electrochemical impedance spectroscopy (EIS) are shown in **Fig. 4**, where the intercepts in the high frequency area correspond to the electrolyte resistance (R_e), the two slightly depressed semicircles in the middle frequency area correspond to the contact resistance (R_1), charge transfer resistance (R_2), and their constant phase elements (CPE), and the inclined lines at low frequency area correspond to the Warburg element (Z_w). Initial electrolyte resistance of 11.27 Ω and contact resistance of 198.6 Ω have shown only small shifts upon cycling to 13.57 Ω and 205.5 Ω after 20 cycles, respectively, while initial charge transfer resistance of 430 Ω has been almost doubled to 820 Ω . Previously reported similar impedance study suggests that dislocations or cracks of the initial framework during charge and discharge processes increase the internal resistances and hinder phase transition kinetics,¹¹ which should be mainly attributable to two phases; pristine NaVP₂O₇ and partially desodiated Na_{1-x}VP₂O₇.

This explains why as-prepared NaVP₂O₇ only reached less than 50% of its theoretical capacity even at low current rate (1/20 C) with relatively high polarization. To investigate further its electrochemical activity, XPS (**Fig. 5**) data were collected to estimate atomic coordination and valence states of P and V. As expected, only small peak shifts in slightly high initial V³⁺ peaks at 518.1 eV (V2p_{3/2}) and 524.5 eV (V2p_{1/2}) to 518.2 eV (V2p_{3/2}) and

524.8 eV ($V2p_{1/2}$) respectively were observed upon charging and the peaks reverted back to their original positions upon discharging. Peak at P 2p core level (135.2 eV) shifted to slightly lowered binding energy of 134.9 eV upon charging and 134.5 eV after the initial cycle, which indicates that the pristine structure undergoes irreversible bond order reduction of phosphorus in P_2O_7 when Na-ion is inserted/extracted by electrochemical means.³³ Meanwhile, weak peak in P 2p core level (137.8 eV) appeared upon desodiation, which could be only observed when the peak was not fitted using two separate background functions. As the known spin-orbit splitting (Δ) between P $2p_{1/2}$ and P $2p_{3/2}$ is rather small (~ 1 eV), this peak should be attributable to trace amount of pure metaphosphate group (PO_3) different from bridged- PO_3 in P_2O_7 group.

To further analyze the XPS results, each sample was characterized by Attenuated total reflectance Fourier transform infrared (ATR-FTIR) spectrometer as illustrated in **Fig. 6**. The doublet symmetric vibration modes of PO_3 were observed at 1034 cm^{-1} and 1053 cm^{-1} , respectively. The symmetric and asymmetric vibration peaks of P-O-P bonds, which are indicative of pyrophosphate group, were observed at 743.2 cm^{-1} and 934 cm^{-1} , respectively. The distinctive peaks below 639 cm^{-1} are attributable to O-P-O bonds.³⁴ The initially observed peaks were maintained upon cycling. However, doublet symmetric vibration modes of PO_3 at 853 cm^{-1} and 838 cm^{-1} were observed after initial charging, which confirms that a part of the bond order for P-O in pyrophosphate group is decreased after Na-extraction, while the rest of P_2O_7 retains their unique vibration modes.³⁵

3.3. Theoretical considerations

DFT calculation can shed crucial insights to understand structural variations in solid phases. NaVP_2O_7 has one crystallographically unique Na and V sites along with two P sites with 4-fold symmetry, generating the centrosymmetric space group of $P2_1/c$. It means the treatment of removing any Na-atom from the lattice structure will break the local symmetry, thereby forcing the initial structure to be noncentrosymmetric. To simulate possible phase transitions and changes in atomic environments, each atom in the same equivalent position was assigned as independent site and the ground-state NaVP_2O_7 ($a = 7.2806 \text{ \AA}$, $b = 7.8217 \text{ \AA}$, $c = 9.5371 \text{ \AA}$, $\beta = 111.8932^\circ$, and $V = 517.005 \text{ \AA}^3$) was calculated as an initial model. In this simulation, Na-atoms in Na(iii) and Na(iv) sites, which were generated by inversion center from Na-atoms in Na(i) and Na(ii) sites, were taken out and then the rest of Na-ions were removed to predict possible peak splitting upon (de)sodiation due to the lowered symmetry as shown in **Fig. 7**. Interestingly, the simulated XRD pattern of $\text{Na}_{0.5}\text{VP}_2\text{O}_7$ ($a = 7.2410 \text{ \AA}$, $b = 7.8319 \text{ \AA}$, $c = 9.4543 \text{ \AA}$, $\beta = 111.626^\circ$, and $V = 498.42 \text{ \AA}^3$) is similar to that of the pristine NaVP_2O_7 except for a slight separation of (-212) peak induced by decreases in β and c -axial length, while the simulated pattern of VP_2O_7 clearly showed the distinctive peak splitting at around 26° , 28° and 30° . Considering this simulation is based on asymmetrical removal of Na-atoms in its ground state, the actual changes in unit cell volume may be much smaller in experimental results than those of the simulated, which explains seemingly the same ex-situ XRD patterns with pristine pattern.

Single vacancy-assisted Na-ion migration was also calculated and the result is shown in **Fig. 8**. To simulate the lowest energy diffusion pathway, the migration path with the

shortest inter Na-ionic distance of 3.383 Å was considered, which resulted in the migration energy barrier of 0.47 eV. The obtained value is in a good agreement with previously reported disodium metal pyrophosphates, Na₂FeP₂O₇ (0.49 eV) and Na₂MnP₂O₇ (0.58 eV).¹² However, this result suggests that the limited electrochemical activity of the title compound is not merely attributable to sluggish Na-ion migration kinetics, but also to high intrinsic resistance induced by Na-extraction from initial framework, which limits the phase transition kinetics between NaVP₂O₇ and VP₂O₇. It is in agreement with the recent study on isostructural NaFeP₂O₇, which is electrochemically inactive regardless of the presence of open tunnels for Na⁺ migration.³⁶

4. Conclusions

Single-phase sodium vanadium pyrophosphate, NaVP₂O₇, was synthesized via conventional solid-state reaction. NaVP₂O₇ adopts a centrosymmetric space group of *P2₁/c*. Reversible Na⁺ (de)insertion involving partial V⁴⁺/V³⁺ redox activity (at 3.4 V vs. Na/Na⁺) was observed in NaVP₂O₇ for the first time. DFT calculation, XPS, FT-IR and ex-situ XRD results show that partial Na-ion extraction brings a slight distortion in the pyrophosphate groups, which accompanies only small changes in lattice structure with lowered symmetry. The single-vacancy assisted migration barrier energy of NaVP₂O₇ calculated by NEB calculation was similar to those of disodium metal pyrophosphates, which itself could not account for low specific capacity of the title compound. However, EIS and galvanostatic charge/discharge data further show that the limited electrochemical

activity of NaVP_2O_7 is associated with intrinsically high resistance, which limits phase transition kinetics between NaVP_2O_7 ($P2_1/c$) and $\text{Na}_{1-x}\text{VP}_2\text{O}_7$ ($P2_1$).

Acknowledgements

This work was financially supported by the Elements Science & Technology Projects of MEXT, Japan.

References

- [1] B. Zhang, X. Ou, J. Zheng, C. Shen, L. Ming, Y. Han, J. Wang, and S. Qin, *Electrochimica Acta*, 2014, **133**, 1.
- [2] M.A.E Sanchez, G.E.S. Brito, M.C.A. Fantini, G.F. Goya, and J.R. Matos, *Solid State Ionics*, 2006, **177**, 497.
- [3] Y. Cui, X. Zhao, and R. Guo, *J. Alloy Compd*, 2010, **490**, 236.
- [4] Y. Kee, N. Dimov, E. Kobayashi, A. Kitajou, and S. Okada, *Solid State Ionics*, 2015, **272**, 138.
- [5] Y. Uebou, S. Okada, M. Egashira, and J. Yamaki, *Solid State Ionics*, 2002, **148**, 323.
- [6] L. Qu, S. Fang, Z. Zhang, L. Yang, and S. Hirano, *Mater. Lett.*, 2013, **108**, 1.
- [7] L. Tan, S. Zhang, and C. Deng, *J. Power Sources*, 2015, **275**, 6.
- [8] S. Zhang, C. Deng, H. Gao, F.L. Meng, and M. Zhang, *Electrochimica Acta*, 2013, **107**, 406.
- [9] Y. Kee, N. Dimov, K. Minami, and S. Okada, *Electrochimica Acta*, 2015, **174**, 516.
- [10] Z. Jian, L. Zhao, H. Pan, Y. Hu, H. Li, W. Chen, and L. Chen, *Electrochem. Commun.*, 2012, **14**, 86.
- [11] Y. Zhu, Y. Xu, Y. Liu, C. Luo, and C. Wang, *Nanoscale*, 2013, **5**, 780.
- [12] J. M. Clark, P. Barpanda, A. Yamada, and M. Islam, *J. Mater. Chem.A*, 2014, **2**, 11807.
- [13] S. Ong, V. Chevrier, G. Hautier, A. Jain, C. Moore, S. Kim, X. Ma, and G. Ceder, *Energy Environ. Sci.*, 2011, **4**, 3680.
- [14] P. Barpanda, S. Nishimura, and A. Yamada, *Adv. Energy Mater.*, 2012, **2**, 841.

- [15] C. Deng, S. Zhang, and Y. Wu, *Nanoscale*, 2015, **7**, 487.
- [16] C. Deng, S. Zhang, Z. Dong, and Y. Shang, *Nano Energy*, 2014, **4**, 49.
- [17] S. Park, I. Gocheva, S. Okada, and J. Yamaki, *J. Electrochem. Soc.*, 2011, **158**, A1067.
- [18] S. Nishimura, M. Nakamura, R. Natsui, and A. Yamada, *J. Am. Chem. Soc.*, 2010, **132**, 13596.
- [19] P. Barpanda, T. Ye, S. C. Chung, Y. Yamada, S. Nishimura, and A. Yamada, *J. Mater. Chem.*, 2012, **22**, 13455.
- [20] J. Barker, R.K.B. Gover, P. Burns, and A. Bryan, *Electrochem. Solid-State Lett.*, 2005, **8**, A446.
- [21] Y.P. Wang and K.H. Lii, *Acta Cryst.*, 1989, **C45**, 1417.
- [22] G. Kresse and J. Furthmüller, *Phys. Rev. B*, 1996, **54**, 11169.
- [23] G. Kresse and D. Joubert, *Phys. Rev. B*, 1999, **59**, 1758.
- [24] G. Henkelman, B.P. Uberuaga, and H. Jónsson, *J. Chem. Phys.*, 2000, **113**, 9901.
- [25] A. Leclaire, M. M. Borel, A. Grandin, and B. Raveau, *J. Solid State Chem.*, 1988, **76**, 131.
- [26] A. Leclaire, A. Benmoussa, M.M. Borel, A. Grandin, and B. Raveau, *J. Solid State Chem.*, 1988, **77**, 299.
- [27] G. Rouse, C. Wurm, M. Morcrette, J. Rodriguez-Carvajal, J. Gaubicher, and C. Masquelier, *Int. J. Inorg. Mater.*, 2001, **3**, 881.
- [28] P. Barpanda, T. Ye, S. Nishimura, S. C. Chung, Y. Yamada, M. Okubo, H. Zhou, and A. Yamada, *Electrochem. Commun.*, 2012, **24**, 116.

- [29] P. Barpanda, T. Ye, M. Avdeev, S. C. Chung, and A Yamada, *J. Mater. Chem. A*, 2013, **1**, 4194.
- [30] N. Meethong, H.-Y.S. Huang, W.C. Carter, and Y.-M. Chiang, *Electrochem. Solid-State Lett.*, 2007, **10**, A134.
- [31] G. Kobayashi, S. Nishimura, M.-S. Park, R. Kanno, M. Yashima, T. Ida, and A. Yamada, *Adv. Funct. Mater.*, 2009, **19**, 395.
- [32] N. Meethong, H.-Y.S. Huang, S.A. Speakman, W.C. Carter, and Y.-M. Chiang, *Adv. Funct. Mater.*, 2007, **17**, 1115.
- [33] A. Majjane, A. Chahine, M. Et-tabirou, B. Echchahed, T. Do, and P.M. Breen, *Mater. Chem. Phys.*, 2014, **143**, 779.
- [34] H. Zhou, S. Upreti, N.A. Chernova, G. Hautier, G. Ceder, and M.S. Whittingham, *Chem. Mater.*, 2011, **23**, 293.
- [35] P. S. Attidekou, P.A. Connor, P. Wormald, D.P. Tunstall, S.M. Francis, and J.T.S. Irvine, *Solid State Ionics*, 2004, **175**, 185.
- [36] P. Barpanda, G. Liu, C. D. Ling, M. Tamaru, M. Avdeev, S. C. Chung, Y. Yamada and, A. Yamada, *Chem. Mater.*, 2013, **25**, 3480.

Figure Captions

Fig. 1 Schematic view of VO_6 octahedra (a), P_2O_7 isolated pyrophosphate units (b), and NaVP_2O_7 (c) along b-axis and the XRD profiles of the observed and calculated pattern for NaVP_2O_7 .

Fig. 2 The first (solid line) and second (dashed line) charge/discharge curves of NaVP_2O_7 measured at $C/20$ rate (a) and its cyclic performance at various C-rates (b) in the voltage range between 2.5 and 4.0 V.

Fig. 3 TEM images of 12 h ball-milled $\text{NaVP}_2\text{O}_7/\text{C}$ (a, b) and partially desodiated $\text{NaVP}_2\text{O}_7/\text{C}$ electrode (c, d).

Fig. 4 Nyquist plots measured before galvanostatic cycling (white circles) and after 20th cycle (black circles). The applied equivalent circuit (upper left) is plotted in solid lines.

Fig. 5 The X-ray photoelectron spectroscopy (XPS) of pristine NaVP_2O_7 (a), after charging (b), and after discharging (c).

Fig. 6 FT-IR spectra of pristine NaVP_2O_7 (a), NaVP_2O_7 after charging (b), and NaVP_2O_7 after discharging (c) between 500 and 1200 cm^{-1} .

Fig. 7 Ex-situ XRD data measured before cycling (a), after charging (b), after initial cycle (c), and the simulated powder X-ray diffraction patterns of NaVP_2O_7 (d), $\text{Na}_{0.5}\text{VP}_2\text{O}_7$ (e), and VP_2O_7 (f).

Fig. 8 The single vacancy-assisted Na-ion diffusion path and corresponding migration energy barrier.

Table 1. Fractional atomic coordinates of the experimentally obtained (a) and the calculated (b) pristine NaVP_2O_7 . Equivalent sites assigned as independent sites for DFT calculation are generated using following symmetry operators: (i) x, y, z , (ii) $-x, y+1/2, -z+1/2$, (iii) $-x, -y, -z$, (iv) $x, -y+1/2, z+1/2$.

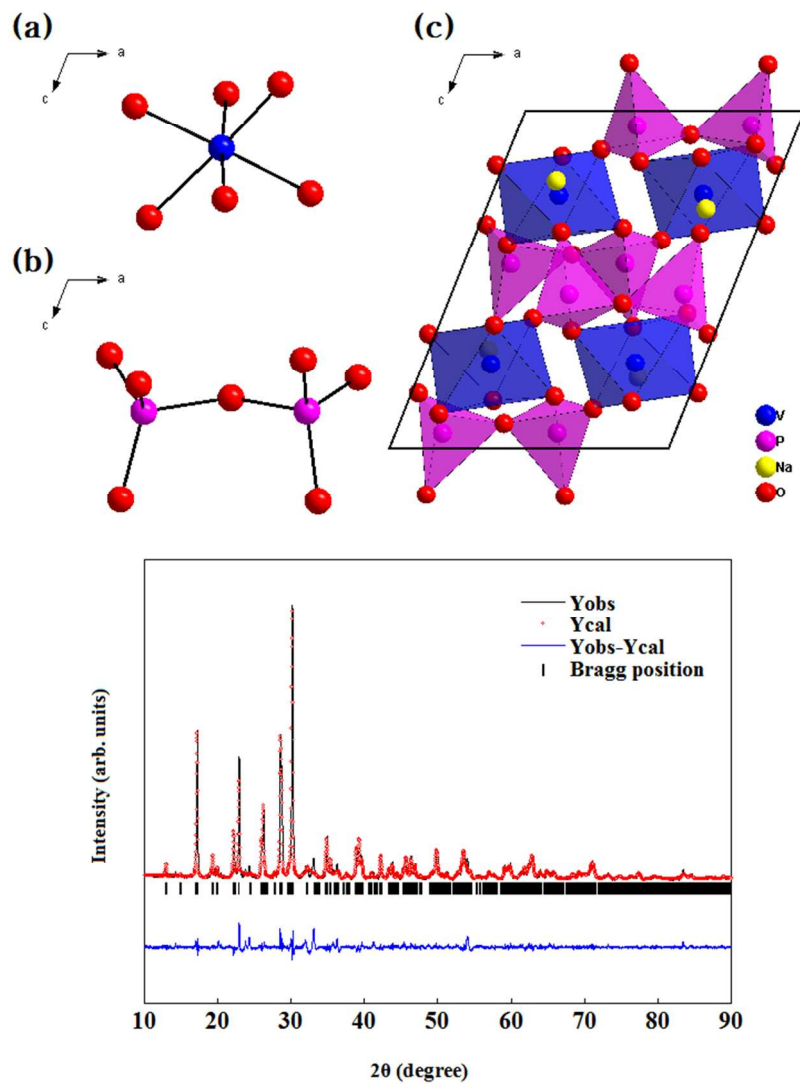


Fig. 1 Schematic view of VO_6 octahedra (a), P_2O_7 isolated pyrophosphate units (b), and NaVP_2O_7 (c) along b -axis and the XRD profiles of the observed and calculated pattern for NaVP_2O_7 .

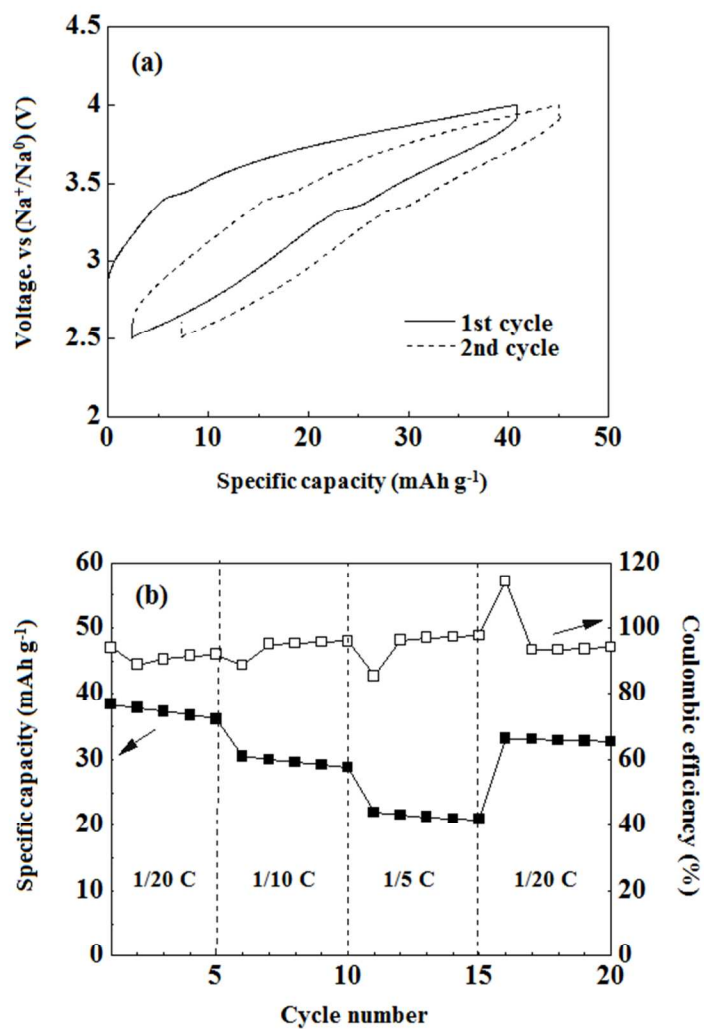


Fig. 2 The first (solid line) and second (dashed line) charge/discharge curves of NaVP₂O₇ measured at C/20 rate (a) and its cyclic performance at various C-rates (b) in the voltage range between 2.5 and 4.0 V.

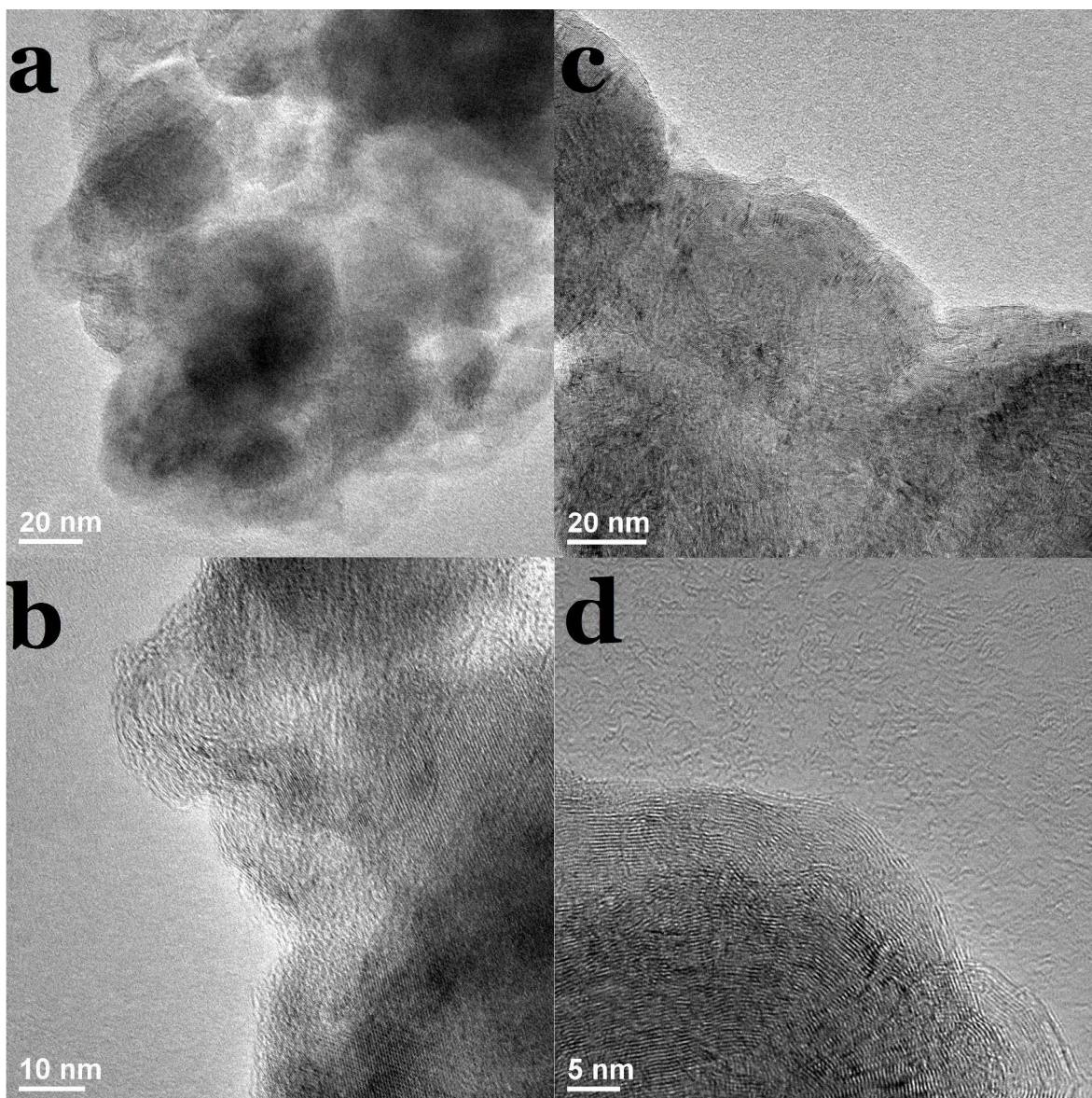


Fig. 3 TEM images of 12 h ball-milled NaVP₂O₇/C (a, b) and partially desodiated NaVP₂O₇/C electrode (c, d).

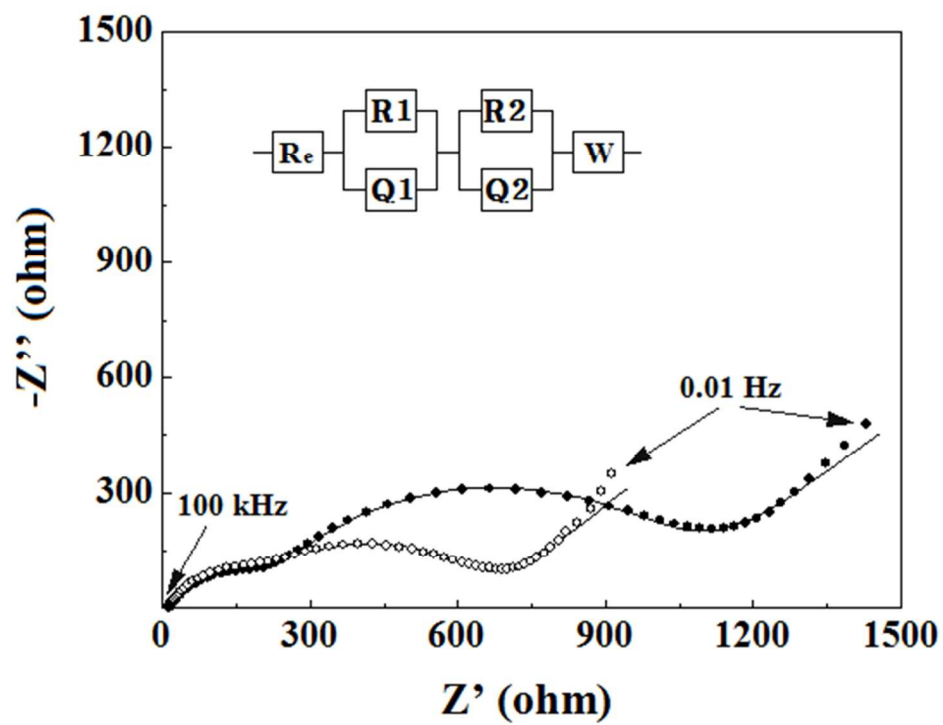


Fig. 4 Nyquist plots measured before galvanostatic cycling (white circles) and after 20th cycle (black circles). The applied equivalent circuit (upper left) is plotted in solid lines.

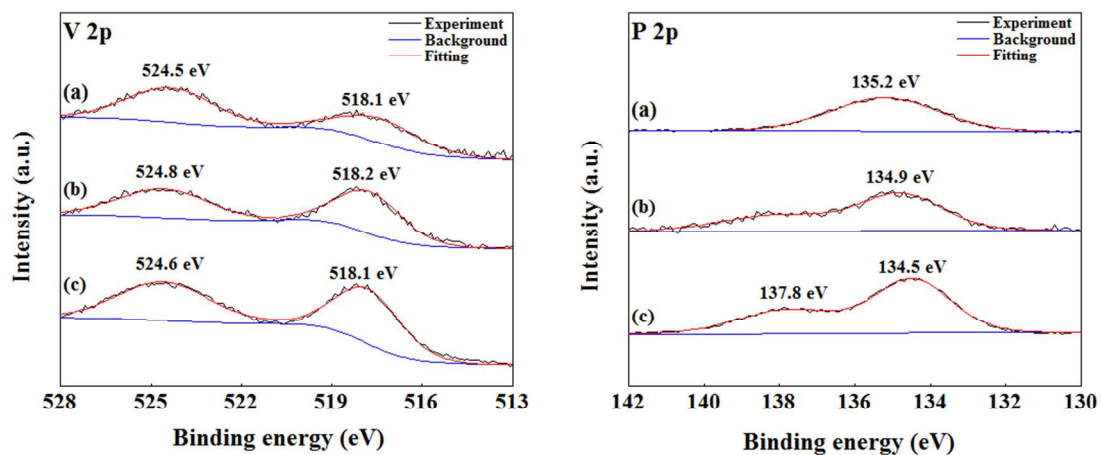


Fig. 5 The X-ray photoelectron spectroscopy (XPS) of pristine NaVP₂O₇ (a), after charging (b), and after discharging (c).

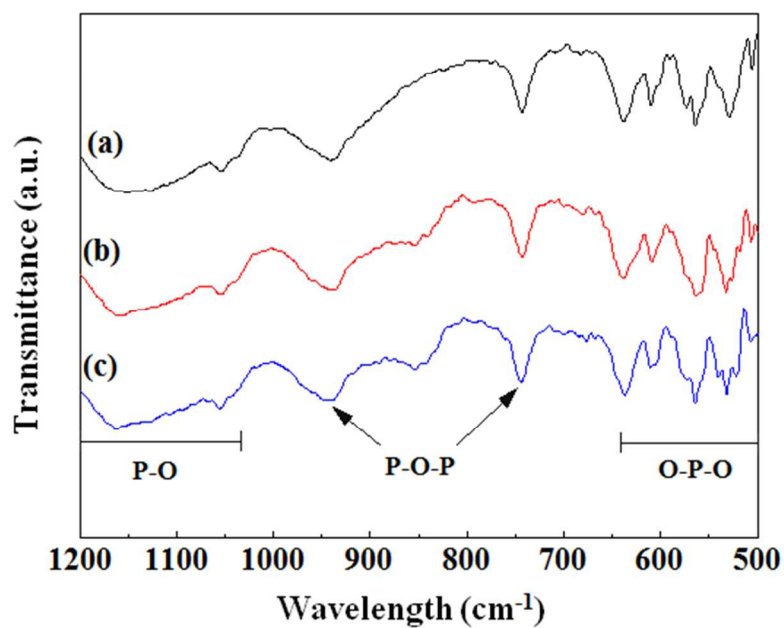


Fig. 6 FT-IR spectra of pristine NaVP₂O₇ (a), NaVP₂O₇ after charging (b), and NaVP₂O₇ after discharging (c) between 500 and 1200 cm⁻¹.

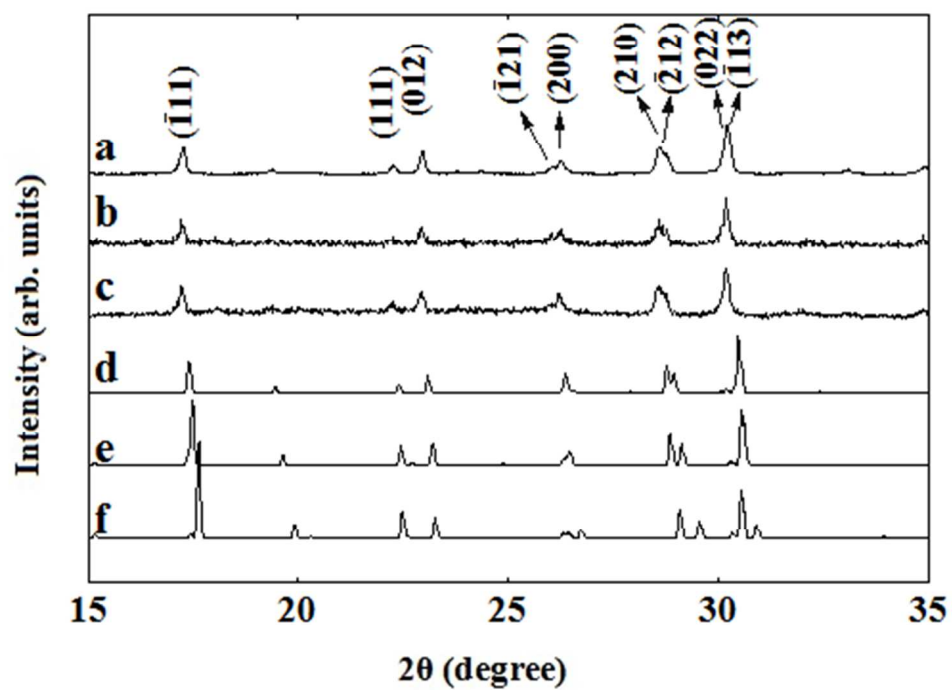


Fig. 7 Ex-situ XRD data measured before cycling (a), after charging (b), after initial cycle (c), and the simulated powder X-ray diffraction patterns of NaVP₂O₇(d), Na_{0.5}VP₂O₇ (e), and VP₂O₇ (f).

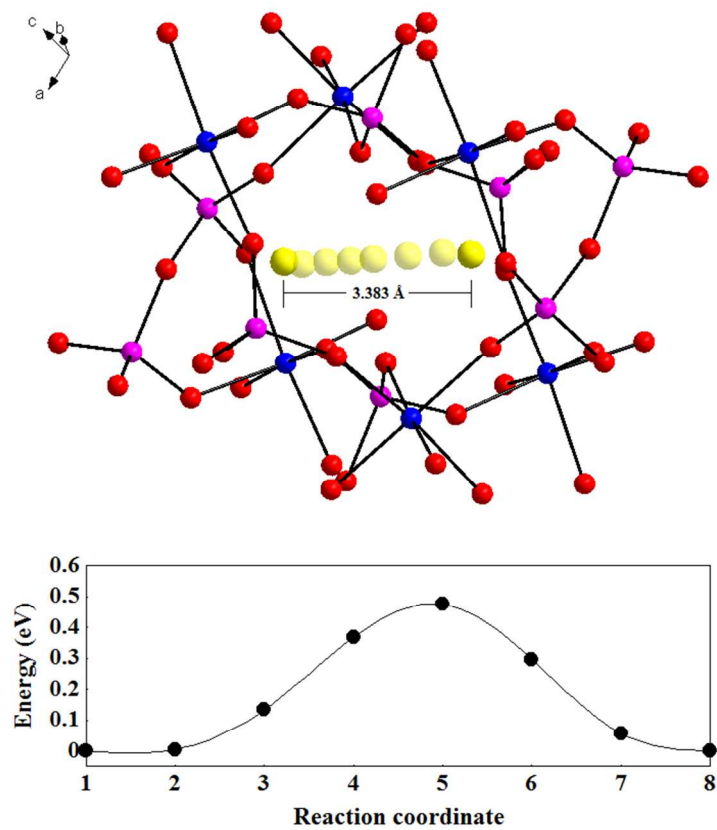


Fig. 8 The single vacancy-assisted Na-ion diffusion path and corresponding migration energy barrier.

Table 1. Fractional atomic coordinates of the experimentally obtained (a) and the calculated (b) pristine NaVP₂O₇. Equivalent sites assigned as independent sites for DFT calculation are generated using following symmetry operators: (i) x, y, z, (ii) -x, y+1/2, -z+1/2, (iii) -x, -y, -z, (iv) x, -y+1/2, z+1/2.

(a)	<i>x</i>	<i>y</i>	<i>z</i>	(b)	<i>x</i>	<i>y</i>	<i>z</i>
V	0.242(3)	0.510(4)	0.252(3)	V	0.2391	0.5074	0.2519
P1	0.168(4)	0.216(4)	0.455(4)	P1	0.1717	0.2139	0.4576
P2	0.578(5)	0.261(5)	0.454(4)	P2	0.5773	0.2550	0.4582
Na	0.212(6)	0.978(5)	0.209(4)	Na	0.2115	0.9806	0.2077
O1	0.517(1)	0.077(8)	0.848(7)	O1	0.5179	0.0799	0.8652
O2	0.198(9)	0.194(8)	0.636(9)	O2	0.1923	0.2056	0.6230
O3	0.303(1)	0.780(1)	0.860(8)	O3	0.3096	0.7814	0.8724
O4	0.374(1)	0.154(8)	0.427(7)	O4	0.3765	0.1545	0.4416
O5	0.025(1)	0.084(8)	0.338(7)	O5	0.0334	0.0841	0.3514
O6	0.128(1)	0.396(9)	0.399(8)	O6	0.1306	0.3991	0.4021
O7	0.673(1)	0.136(9)	0.384(8)	O7	0.6885	0.1323	0.3980